Weierstraß-Institut
für Angewandte Analysis und Stochastik

im Forschungsverbund Berlin e. V.

Preprint ISSN 0946 – 8633

Dynamical regimes in a monolithic passively mode-locked quantum dot laser

Andrei G. Vladimirov[1], Uwe Bandelow [1], Gerrit Fiol[2], Dejan Arsenijević[2], Moritz Kleinert[2], Dieter Bimberg[2] , Alexander Pimenov[3], Dmitrii Rachinskii[3]

submitted: 9 June 2010

[1] Weierstrass Institute
for Applied Analysis and Stochastics
Mohrenstr. 39
10117 Berlin, Germany
E-Mail: vladimir@wias-berlin.de
bandelow@wias-berlin.de

[2] Institut für Festkörperphysik
Technische Universität Berlin
Hardenbergstr. 36, 10623 Berlin
Germany
E-mail: gerrit.fiol@physik.tu-berlin.de
dejan@sol.physik.tu-berlin.de
moritz.kleinert@physik.tu-berlin.de
bimberg@physik.TU-Berlin.DE

[3] Dept. of Applied Mathematics
University College Cork, Ireland
E-mail: d.rachinskii@ucc.ie

No. 1517
Berlin 2010

2010 *Mathematics Subject Classification.* 78A60, 65P30.

Key words and phrases. Mode-locking, quantum dot lasers, bifurcations.

1999 *Physics and Astronomy Classification Scheme.* 42.60.Fc, 042.55.Px, 42.65.S.

Edited by
Weierstraß-Institut für Angewandte Analysis und Stochastik (WIAS)
Mohrenstraße 39
10117 Berlin
Germany

Fax: +49 30 2044975
E-Mail: preprint@wias-berlin.de
World Wide Web: http://www.wias-berlin.de/

Abstract

Operation regimes of a two section monolithic quantum dot (QD) mode-locked laser are studied experimentally and theoretically, using a model that takes into account carrier exchange between QD ground state and 2D reservoir of a QD-in-a-well structure, and experimentally. It is shown analytically and numerically that, when the absorber section is long enough, the laser exhibits bistability between laser off state and different mode-locking regimes. The Q-switching instability leading to slow modulation of the mode-locked pulse peak intensity is completely eliminated in this case. When, on the contrary, the absorber length is rather short, in addition to usual Q-switched mode-locking, pure Q-switching regimes are predicted theoretically and observed experimentally.

1 Introduction

Mode-locking (ML) in lasers is a powerful tool for generating short optical pulses for different practical applications ranging from high speed communication to medical diagnostics. In particular, monolithic passively mode-locked semiconductor lasers are compact sources of picosecond pulses with high repetition rates suitable for applications in telecommunication technology [1, 2]. Recently a new generation of mode-locked semiconductor lasers based on quantum-dot (QD) material was developed [3]. These lasers demonstrate many advantages over conventional quantum well lasers, such as low threshold current, small alpha factor [4], low pulse chirp, high stability to noise and external feedback, etc. [5, 6]. It was recently shown that QD mode-locked lasers can generate very short subpicosecond optical pulses [7, 8].

Due to the discrete nature of electronic states in QD lasers, they demonstrate a number of characteristic features distinguishing them from conventional semiconductor devices [9]. Therefore, theoretical modeling of these lasers requires development of more sophisticated tools, which take into account these features. In particular, carrier dynamics in quantum dot lasers must include carrier exchange processes between 2D reservoir of a QD-in-a-well structure [10, 10] and the discrete levels in quantum dots. These processes are characterized by a large number of quite different characteristic time scales, which have an important impact on the quality of mode-locked pulses and the dynamical behavior of the laser in general.

Rate equations describing the carrier exchange dynamics in QD lasers were proposed in [11, 12, 10]. These equations govern the time evolution of three quantities: carrier density in the 2D reservoir and occupation probabilities of two discrete levels in quantum dots, corresponding to the first excited state and the ground state, respectively.

Assuming that the carrier relaxation rate from the excited states to the ground state is sufficiently fast one gets only two rate equations for the occupation probability ρ of the quantum dot ground state and the carrier density n in the 2D reservoir [13, 14]. Similar pairs of carrier rate equations for gain and absorber sections were recently incorporated into the delay differential model to describe passive ML in quantum dot lasers [15, 16]. It was shown that fast carrier capturing from the 2D reservoir to quantum dots can lead to suppression of the undesirable Q-switching instability of the fundamental ML [14]. Such instability leading to a degradation of the quality of the ML regime is quite difficult to eliminate in quantum well mode-locked devices [2, 17]. In this paper, using the delay differential equations (DDE) model [16] together with traveling wave equations [18], we perform a more systematic study of the effect of carrier exchange processes on the dynamics of a quantum dot mode-locked laser. We show theoretically, that taking into consideration Pauli blocking in carrier exchange terms can lead to a qualitative change in the laser dynamical behavior. When the absorber section is long enough the Q-switching instability of fundamental ML regime disappears and bistability appears between the laser off state and different ML regimes. We also describe the period doubling bifurcation of a harmonic ML regime leading to different amplitudes and separations of two pulses circulating in the cavity. In a laser with relatively short absorber section the Q-switching instability in the ML regime takes place at sufficiently small injection currents. In this case we show theoretically and confirm experimentally that at sufficiently small injection currents and reverse biases applied to the absorber section, apart from usual Q-switched ML the laser can operate in a pure Q-switching regime.

2 Model equations

We consider a model of passively mode-locked quantum-dot laser consisting of two sections, a forward biased amplifying section and a reversely biased saturable absorber section. In each section the spatial-temporal evolution of the amplitudes of two counter-propagating waves $E^{\pm}$ can be described by the so-called traveling wave equations [18, 19]:

$$\frac{\partial E^{\pm}}{dt} \pm \frac{\partial E^{\pm}}{\partial z} = -\frac{\beta_{g,q}}{2} E^{\pm} + \frac{g_{g,q}}{2}(2\rho - 1)E^{\pm}, \tag{1}$$

where the index g corresponds to the amplifying section and the index q refers to the absorber section. The parameters $\beta_{g,q}$ describe linear internal losses in the semiconductor medium and g_g (g_q) is the differential gain (loss) parameter in the amplifying (absorbing) section. In Eqs. (1) for the sake of simplicity we have neglected the dependence of the refractive index of the semiconductor medium on the occupation probabilities of QD levels and carrier density in the 2D reservoir. Assuming that the relaxation of populations from upper QD levels to the ground state is fast enough, we use the following equations to describe carrier exchange processes between quantum dots and 2D reservoir [13, 14]:

$$\frac{\partial \rho}{\partial t} = -\gamma_{g,q}\rho - r_{g,q}\rho + b_{g,q}n(1-\rho) - g_{g,q}(2\rho-1)\left(|E^{+}|^{2}+|E^{-}|^{2}\right), \tag{2}$$

$$\frac{\partial n}{\partial t} = \eta_{g,q} - \delta_{g,q}n + 2r_{g,q}\rho - 2b_{g,q}n(1-\rho). \tag{3}$$

Here ρ is the QD ground state occupation probability and n, is the carrier density in the 2D reservoir. The factor 2 in Eq. (3) accounts for the double degeneracy of the ground state in quantum dots. The parameters $\gamma_{g,q}$ ($\delta_{g,q}$) are the inverse radiative lifetimes in the quantum dots (inverse effective residence times in the 2D reservoir). The parameters $r_{g,q}$ and $b_{g,q}$ describe, respectively, the rate of carrier escape from quantum dots to the 2D reservoir and the carrier capture rate from the reservoir to the quantum dots. The term η_g in Eq. (3) describes linear gain due to injection current. Since there is no injection current in the absorber section, we have $\eta_q = 0$. However, we assume that the relaxation time δ_q increases with the increase of the reverse voltage applied to the absorber section. Boundary conditions for Eqs. (1) are given by $E^{+}(0,t) = \sqrt{\kappa_1}E^{-}(0,t)$ and $E^{-}(L,t) = \Gamma\sqrt{\kappa_2}\int_0^{\infty} e^{-\Gamma\tau}E^{+}(L,t-\tau)\,d\tau$, where $z=0$ ($z=L$) corresponds to the left (right) laser facet. These conditions account for the reflectivities of the facets $\kappa_{1,2}$ and the gain dispersion which is described by Lorentzian filter of width Γ [20].

Equations (1)-(3) have been used for numerical modeling of dynamics in monolithic quantum dot lasers. A numerical scheme for solving these equations is described in [20]. Along with these equations a simplified model assuming ring cavity geometry and unidirectional lasing approximation [15, 16, 21] was used. This model can be written as a set of five delay differential equations [14]

$$\Gamma^{-1}\frac{dA}{dt} + A = \sqrt{\kappa}e^{G(t-T)/2+Q(t-T)/2}A(t-T), \tag{4}$$

$$\frac{dP_g}{dt} = -(\gamma_g + r_g)P_g + b_gN_g(1-P_g) - e^{Q}(e^{G}-1)|A|^2, \tag{5}$$

$$\frac{dP_q}{dt} = -\left(\gamma_q + r_q\right)P_q + b_qN_q\left(1-P_q\right) - s(e^{Q}-1)|A|^2, \tag{6}$$

$$\frac{dN_g}{dt} = \delta_g(g_0 - N_g) + 2r_gP_g - 2b_gN_g(1-P_g), \tag{7}$$

$$\frac{dN_q}{dt} = -\delta_qN_q + 2r_qP_q - 2b_qN_q\left(1-P_q\right). \tag{8}$$

Here A is the normalized electric field envelope at the entrance of the absorber section. The variables $P_{g,q} = \int_{g,q}\rho\, dl/l_{g,q}$ and $N_{g,q} = \int_{g,a} n\, dl/l_{g,q}$ are normalized integrals of the occupation probability ρ and carrier density n along the corresponding section, where l_g (l_q) denotes the length of the gain (absorber) section. Cumulative saturable gain G and loss Q introduced by the gain and absorber sections are given by

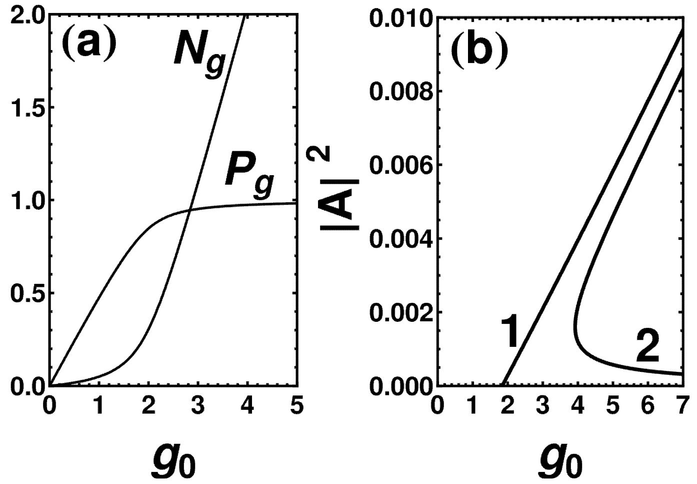

Figure 1: Left: Dependence of the integral carrier density in the 2D reservoir N_g and occupation probability in quantum dots P_g in the gain section on the injection parameter g_0 for the solution with zero laser intensity. Right: Dependence of the laser intensity on the injection parameter g_0. 1 – monostable behavior, short absorber section $l_g = 0.9$ mm, $l_q = 0.1$ mm. 2 – bistable behavior, longer absorber section, $l_g = 0.8$ mm, $l_q = 0.2$ mm. Other parameters are $T = 25$ ps, $s = 15$, $\Gamma^{-1} = 0.4$ ps, $\kappa = 0.3$, $\gamma_g^{-1} = 1$ ns, $\gamma_q^{-1} = 1$ ns, $\delta_g^{-1} = 1$ ns, $\delta_q^{-1} = 10$ ps, $g_g = 4$ mm^{-1}, $g_q = 10$ mm^{-1}, $b_g^{-1} = 5$ ps, $b_q^{-1} = 5$ ps, $r_g^{-1} = 100$ ps, $r_q^{-1} = 10$ ps.

$G = g_g l_g (2P_g - 1)$ and $Q = g_q l_q \left(2P_q - 1\right)$. The parameter T is the cavity round trip time, Γ is the spectral filtering width, κ is the attenuation factor that accounts for the linear nonresonant losses $\beta_{g,q}$ and reflectivities of the laser facets $\kappa_{1,2}$. $g_0 = \int_g \eta_g dl/l_g$ is the injection parameter. Finally, the parameter $s = g_g/g_q$ in (6) is the ratio of the differential gain in the gain section and the differential absorption in the absorber section.

3 CW regimes

In this section we study the solutions of Eqs. (4)-(8) corresponding to cw laser output. The simplest cw solution is that corresponding to zero laser intensity. It is given by

$$A = 0, P_g = P_{g0}, N_g = N_{g0}, P_q = N_q = 0 \tag{9}$$

with

$$P_{g0} = \frac{1+\xi}{2} - \sqrt{\left(\frac{1+\xi}{2}\right)^2 - \frac{g_0\zeta}{2}}, \quad N_{g0} = g_0 - \frac{2P_{g0}}{\zeta}, \tag{10}$$

and

$$\xi = \frac{\zeta}{2}\left(g_0 + \frac{r_g + \gamma_g}{b_g}\right), \quad \zeta = \frac{\delta_g}{\gamma_g}. \tag{11}$$

The dependence of the quantities $P_g = P_{g0}$ and $N_g = N_{g0}$ on the injection parameter g_0 in the amplifying section is shown in Fig. 1a. We see that unlike the integral carrier density N_g in the 2D reservoir, which grows linearly at large injections g_0, the growth of the occupation probability P_g of quantum dots saturates at $P_g = 1$ when the injection current becomes sufficiently large. The smaller the ratio $(r_g + \gamma_g)/b_g$ in (11) and the larger ζ, the faster P_g saturates. This saturation is related to the presence of the Pauli blocking factor $1 - P_g$ in the capture rate term in Eq. (6), hence it is a consequence of the fact that the number of free places for electrons in quantum dots is limited. Saturation of the occupation probability results in saturation of the gain in the amplifying section. This gain can not exceed the maximal value $G = g_g l_g$ corresponding to a state with fully occupied quantum dots, $P_g = \rho_g = 1$.

Since at $A = 0$ the absorber section is completely unsaturated, we have $P_q = 0$ and, hence, the cumulative loss introduced by this section is $Q = -g_q l_q$. Therefore, for $g_0 \to \infty$ when all the states in quantum dots are fully occupied, i.e., $G = g_g l_g$, the stability of the zero intensity cw solution (9)-(11) is determined by the inequality $g_g l_g - g_q l_q + \ln\kappa < 0$, where $\ln\kappa$ describes the linear nonresonant losses. This inequality ensures that the absolute value of the coefficient by the delayed electric field term in Eq. (4) is less than 1. From this condition we see that when the absorber section length is large enough, namely

$$g_q l_q > g_g l_g + \ln\kappa, \tag{12}$$

the zero intensity steady state (9)-(11) remains stable at arbitrary large injection currents (arbitrary large g_0). In this case the maximal achievable linear cumulative gain $G = g_g l_g$ is smaller than total unsaturated losses $|Q| = g_q l_q$ introduced by the absorber section plus linear nonsaturated losses $-\ln\kappa$. However, even in this case laser generation is possible in a regime with strongly saturated absorber. Indeed, in the limit $g_0 \to \infty$ one obtains that apart from zero intensity steady state (9)-(11) there exist two cw solutions with $|A|^2 \neq 0$. The first of these cw solutions corresponds to a fully saturated absorber $P_q = 1/2$ and is always stable in this limit (see the upper branch of curve 2 in Fig. 1b). The second (unstable) solution, see the lower branch of curve 2 in Fig. 1b), corresponds to positive occupation probability $P_q = (g_q l_q - g_g l_g - \ln\kappa)/(2 g_q l_q) > 0$ only when the inequality (12) is satisfied. Otherwise, this solution corresponds to negative occupation probability, $\rho_q < 0$, and laser intensity, $|A|^2 < 0$, and, therefore, is nonphysical. Thus, if the inequality (12) holds, the branch of nonzero-intensity cw solutions is isolated from the zero intensity state (curve 2 in Fig. 1b) and the bistability exists between the two cw states: one with zero and the other with positive laser intensity. If the absorber section length is sufficiently short, so that the inequality (12) is not satisfied, the solution with nonzero laser intensity bifurcates from the zero intensity state at gain parameter value

$$g_0 = \left(g_g l_g + g_q l_q - \ln\kappa\right)\left[\frac{1}{g_g l_g \zeta} + \frac{r_g + \gamma_g}{b_g\left(g_g l_g - g_q l_q + \ln\kappa\right)}\right],$$

which corresponds to the linear lasing threshold (see curve 1 in Fig. 1b). In this case, either there is no bistability or the bistability domain is rather small.

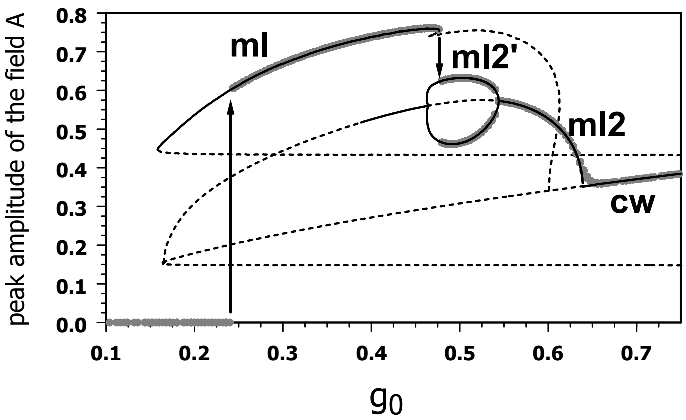

Figure 2: Bifurcation diagram illustrating the sequence of dynamical regimes that takes place with the increase of the injection parameter g_0. Stable (unstable) solutions are shown by solid (dotted) lines. cw, ml, ml2, correspond to continuous wave, fundamental ML, harmonic ML regimes, respectively. ml2' indicates the harmonic ML regime with two different pulses. Gray dots indicate the extrema of the absolute value of the electric field amplitude $|A|$ obtained by means of direct numerical simulation of Eqs. (4)-(8). $\Gamma^{-1} = 0.5$ ps, $l_g = 0.8$ mm, $l_q = 0.2$ mm, $g_g = 2.22$ mm^{-1}, $g_q = 20$ mm^{-1}, $\delta_q^{-1} = 10$ ps, $b_g^{-1} = 1$ ps, $b_q^{-1} = 20$ ps, $r_g^{-1} = 1$ ns, $r_q^{-1} = 10$ ps. Other parameters are the same as for Fig. 1b. Arrows indicate jumps between different regimes.

4 Mode-locking regimes

The results of numerical bifurcation analysis of Eqs. (4)-(8) performed using the path following software package DDEBIFTOOL [22] and direct numerical simulations [23] are summarized in Figs. 2 and 5. These figures show the dependence of the laser field peak intensity on the injection parameter g_0 in lasers with two different lengths of the absorber section.

Long absorber section

Bifurcation diagram shown in Fig. 2 corresponds to a laser with rather long absorber section when the branch of nonzero intensity cw solutions is isolated from laser off state (see Fig. 1b). In Fig. 2 the stable parts of the branches of fundamental (ml) and harmonic (ml2, ml2') ML regimes coexist with the stable laser off state. The lower unstable part of the fundamental ML branch extends to infinite values of g_0. Furthermore, the Q-switching instability of the ML regime does not appear. Thus, by increasing the absorber section length the Q-switching instability can be completely eliminated.

Figure 2 demonstrates another peculiar feature of Eqs. (4)-(8) describing a mode-locked QD laser. For certain parameter values these equations can exhibit a period-doubling bifurcation of the harmonic mode-locked solution with the pulse repetition rate twice larger than that of the fundamental regime. After this bifurcation of the ML

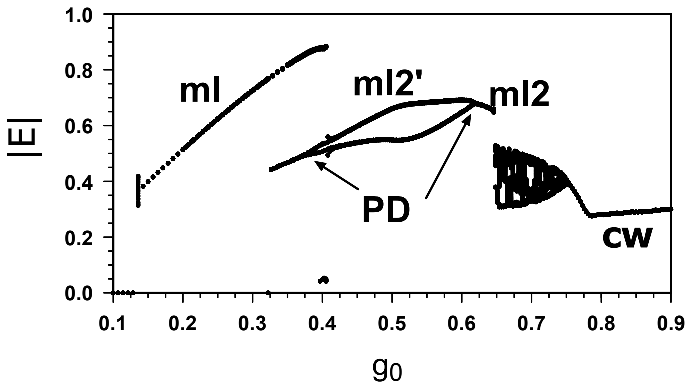

Figure 3: Bifurcation tree obtained by numerical simulation of Eqs. (1)-(3). Black dots correspond to maxi-+*ma of intensity time traces calculated at different values of the injection parameter $g_0 = \eta_g l_g$. Period doubling bifurcations of the harmonic ML regime are labeled PD. $l_g = 1.125$ mm, $l_q = 0.125$ mm, $\Gamma^{-1} = 0.25$ ps, $\kappa_{1,2} = 0.55$, $\beta_g = \beta_q = 0$, $g_g = 2$ mm^{-1}, $g_q = 9$ mm^{-1}, $r_g^{-1} = 20$ ps, $r_q^{-1} = 1$ ns, $\gamma_g^{-1} = \gamma_q^{-1} = 1$ ns, $\delta_g^{-1} = 1$ ns, $\delta_q^{-1} = 10$ ps.

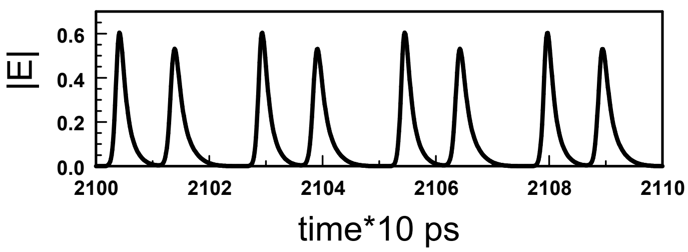

Figure 4: Harmonic ML regime with two pulses having different peak intensities and separations. $g_0 = \eta_g l_g = 0.5$. Other parameters are the same as for Fig. 3.

regime with two pulses circulating in the cavity, the pulses acquire different amplitudes and separations. This regime is indicated ml2' in Fig. 2. Similar period-doubling bifurcation was found in numerical simulations of the traveling wave equations (1)-(3), see the bifurcation diagram in Fig. 3, which is qualitatively very similar to that in Fig. 2, and time trace in Fig. 4. A regime with two different pulses existing in the cavity simultaneously was recently observed experimentally in a 20 GHz two-section mode-locked QD laser [24]. The period doubling bifurcation shown in Figs. 2 and 3 is different from that described in Ref. [20] for a mode-locked quantum well laser. The latter bifurcation is possible only in the case of the linear cavity geometry when an additional passive section is present in the laser cavity. This contrasts to the period doubling bifurcation shown in Fig. 2, which appears in the DDE model (4)-(8) of a two section laser assuming a ring laser cavity. This bifurcation may be attributed to a more complicated carrier dynamics in the QD laser model (4)-(8) as compared to the models [15, 16, 21, 20] of quantum well lasers.

Short absorber section

Figure 5 presents a diagram similar to that of Fig. 2, but corresponding to a shorter absorber section. The bifurcation sequence depicted in this figure is qualitatively similar to that described earlier for a model of a monolithic quantum well mode-locked device [15, 16]. ML solutions bifurcate from the cw solution corresponding to nonzero laser intensity. At sufficiently small injection currents g_0 the fundamental ML regime exhibits an instability towards a regime with undamped oscillations of the pulse peak intensity at the Q-switching frequency. This regime of "Q-switched" ML is indicated qsml in Fig. 5 (see also the time trace in Fig. 6b). However, unlike the model of quantum well laser described in [15, 16], the QD ML model (4)-(8) apart from Q-switched ML can exhibit a pure Q-switching regime. In the latter regime, indicated qs in Fig. 5, the laser emits a sequence of pulses with the repetition frequency of the order of 1 GHz. The corresponding time trace and power spectrum are shown in Fig. 6c. With the increase of the injection current the Q-switching regime looses stability and a transition to Q-switched ML with quasiperiodic laser intensity takes place, as it is illustrated by Fig. 6b. At even higher injection currents, the fundamental ML regime labeled ml becomes stable. This regime is characterized by a sequence of short pulses with the repetition period close to the cavity round trip time and a single peak at the frequency close to 40 GHz in the power spectrum, see Fig. 6c. With further increase of the injection parameter g_0, transitions to harmonic ML regime with approximately twice higher repetition rate and finally to a stable cw regime take place. These regimes are labeled ml2 and cw in Fig. 5.

Two-parameter plots illustrating the dependence of the ML range on the capture and escape rates in the gain and absorber sections are presented in Figs. 7 and 8. They have been obtained by direct numerical solution of Eqs. (4)-(8). In these figures different dynamical regimes are indicated by different gray levels. As we see from the upper panel of Fig. 7, the range of stable fundamental ML (shown by dark gray) increases

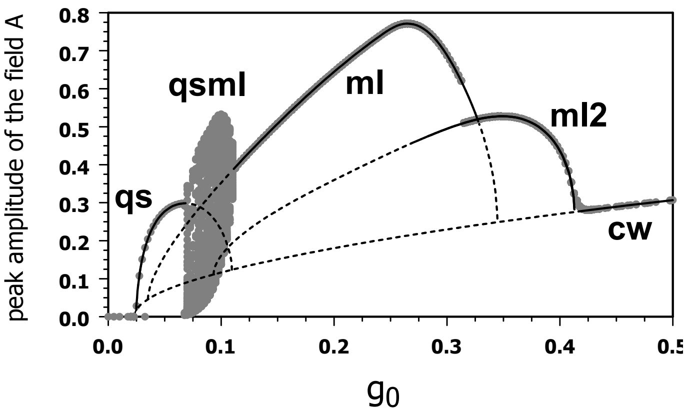

Figure 5: Same as Fig. 2, but calculated for twice shorter absorber section. Solid (dotted) lines correspond to stable (unstable) solutions. cw, ml , ml2, qs, and qsml correspond to continuous wave, fundamental ML, harmonic ML, Q-switching, and Q-switched ML regimes, respectively. ml2' indicates the harmonic ML regime with two different pulses. $l_g = 0.9$ mm, $l_q = 0.1$ mm, $g_g = 4$ mm^{-1}, $g_q = 20$ mm^{-1}, $\delta_q^{-1} = 5$ ps, $r_g^{-1} = 250$ ps, $r_q^{-1} = 6.67$ ps. Other parameters are the same as for Fig. 1b.

with the capture rate b_g in the gain section. However, this dependence is quite weak: the ordinate axis in this figure uses logarithmic scale. The dependence of ML range on the escape rate r_g in the gain section is, on the contrary, quite strong. As it is seen from the lower panel of Fig. 7, the laser can exhibit stable ML only if the carrier escape rate from quantum dots to the 2D reservoir is sufficiently small. With the increase of this rate ML regime is replaced by either a cw or a Q-switching behavior. Figure 8 illustrates the dependence of the ML range on the capture and escape rates in the absorber section. According to this figure the range of fundamental and harmonic ML regimes increases with the decrease of the capture rate b_q and increases with the escape rate r_q. The increase of the ML range is usually accompanied by the appearance of harmonic ML with the pulse repetition rate close to twice the cavity round trip time. However, as it is seen from the lower panel of Fig. 8, when the escape rate r_q to the 2D reservoir becomes significantly larger then the reservoir relaxation rate δ_q the ML range starts to decrease with r_q. Speaking more generally, stable ML is possible only if the relaxation rate δ_q and the escape rate r_q are large enough, i.e., the quantum dot absorber is sufficiently fast. This is in agreement with the classical results of the ML theory [25]. At very small δ_q and/or r_q only Q-switching behavior is possible. We note that these two quantities increase with the reverse bias applied to the absorber section [26].

Fig. 9 illustrates the dependence of the ML range the relaxation rate δ_q, which is the inverse of the effective residence time in the 2D reservoir. The result here is quite similar to that obtained earlier for a quantum well mode-locked laser [16, 17, 19], except for the existence of pure Q-switching regime at small values of δ_q, which correspond to small absolute values of the reverse bias applied to the absorber section. The ML domain increases with the absorber relaxation rate and harmonic ML regimes appear.

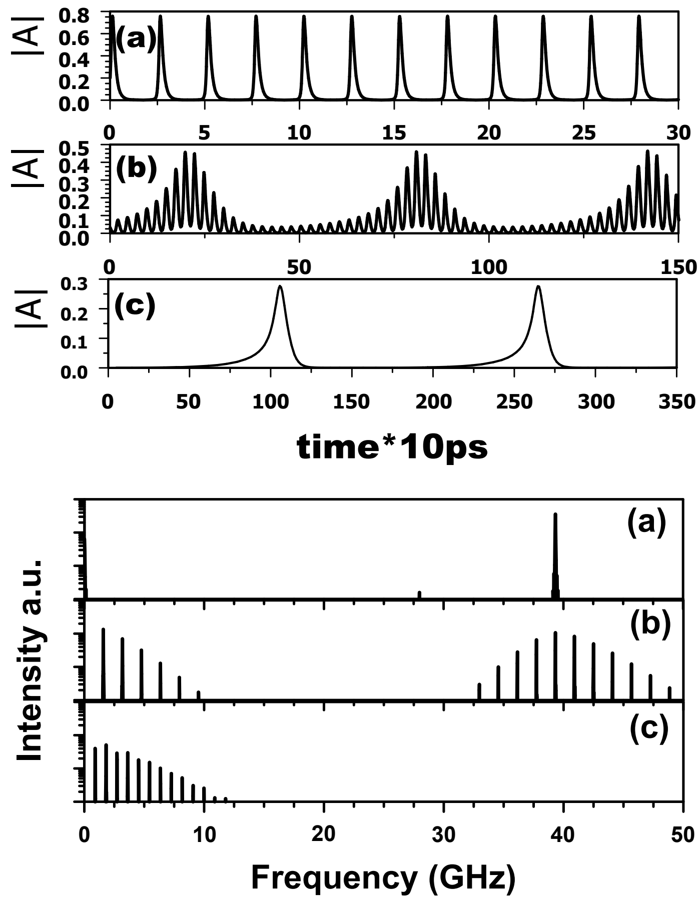

Figure 6: Field amplitude time traces (top) and power spectra (bottom) illustrating dynamical regimes shown in Fig. 5. (a) – fundamental ML (ml); (b) – Q-switched ML (qsml); (c) – pure Q-switching (qs).

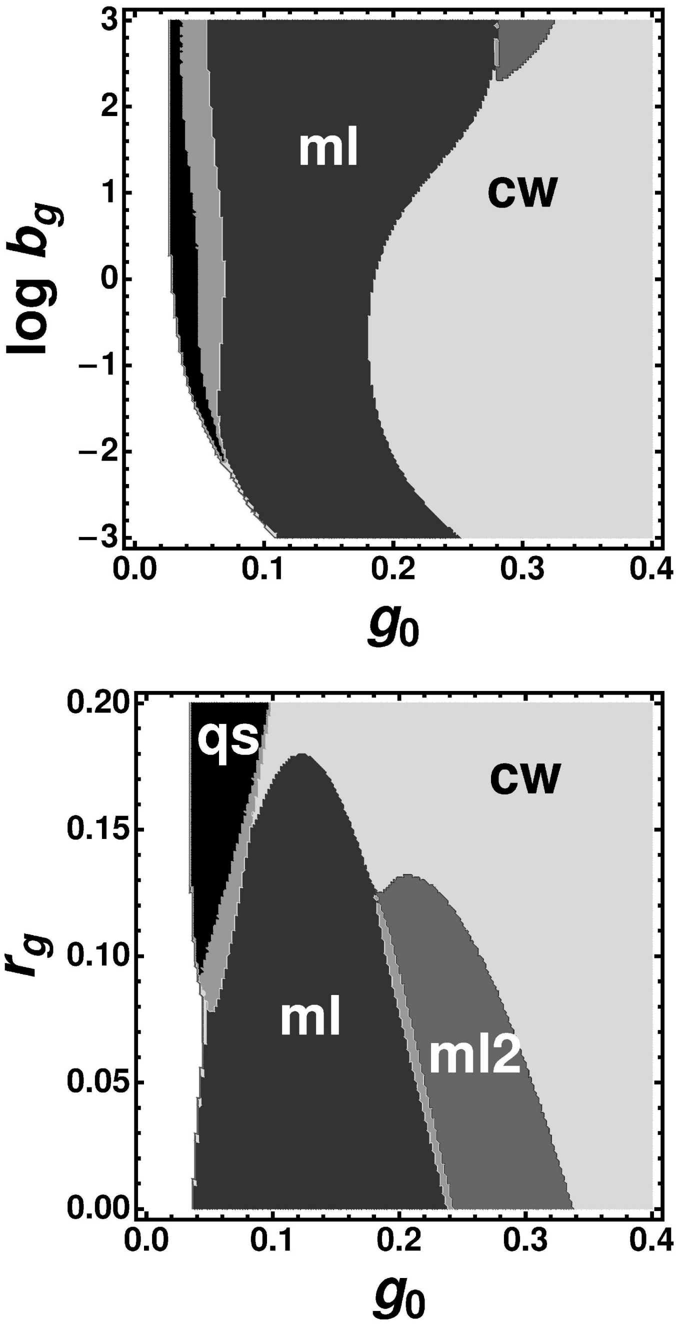

Figure 7: Regions of different dynamical states in the plane of two parameters, capture (b_g) and escape (r_g) rates in the gain section. Different dynamical regimes are indicated by different levels of gray color. White, light gray, dark gray, gray, and black areas indicate, respectively, laser off, continuous wave (cw), fundamental ML (ml), harmonic ML (ml2), and Q-switching (qs) regimes. Gray area between fundamental ML and Q-switching domains corresponds to Q-switched ML regime (qsml). $s = 15$, $\gamma_q^{-1} = 10$ ps. Upper (lower) panel corresponds to $r_g^{-1} = 250$ ps and $r_q^{-1} = 5$ ps ($b_g^{-1} = 5$ ps and $r_q^{-1} = 2.5$ ps). Other parameters are the same as in Fig. 1b.

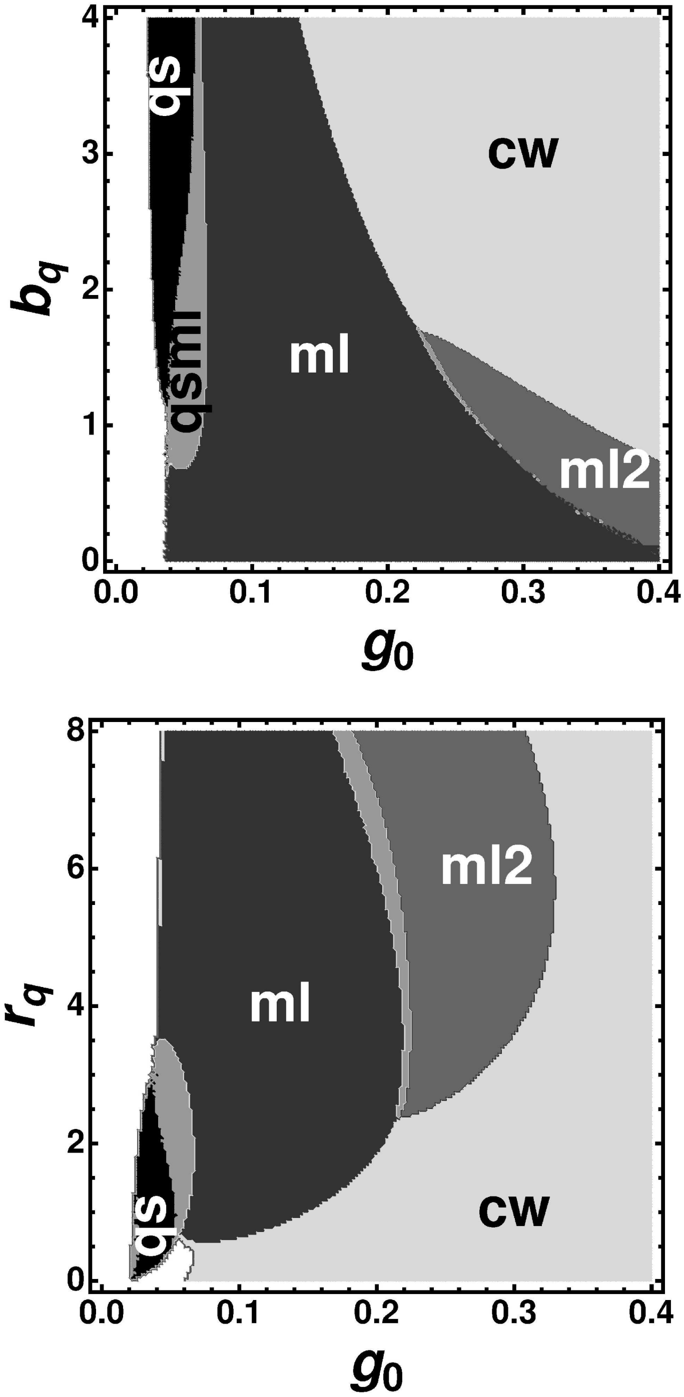

Figure 8: Regions of different dynamical states in the plane of two parameters, capture (b_q) and escape (r_q) rates in the absorber section. Notations are the same as in Fig. 7: ml – fundamental ML regime, ml2 – harmonic ML with approximately twice higher repetition rate, qs – Q-switching, qsml – Q-switched ML, cw – continuous wave regime. $b_g^{-1} = 5$ ps, $r_g^{-1} = 250$ ps. Upper (lower) panel corresponds to $r_q^{-1} = 5$ ps ($b_q^{-1} = 5$ ps). Other parameters are the same as in Fig. 7.

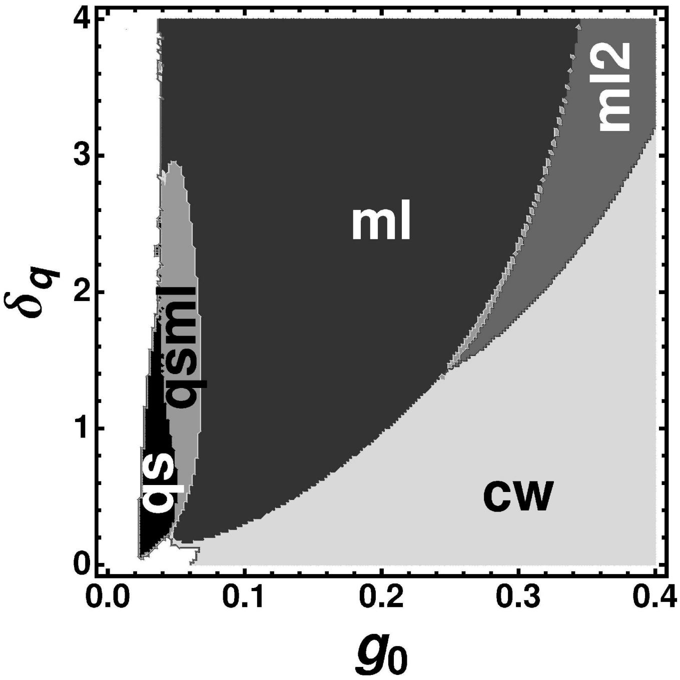

Figure 9: Regions of different dynamical states in the plane of two parameters, injection parameter g_0 and absorber 2D reservoir relaxation rate δ_q. Notations are similar to those of Fig. 7: ml – fundamental ML regime, ml2 – harmonic ML with approximately twice higher repetition rate, qs – Q-switching, qsml – Q-switched ML, cw – continuous wave regime. Parameters are the same as in Fig. 8.

Experiment

Experimental studies have been performed with a ridge waveguide two section QD monolithic mode locked laser. The device dimensions were 4μm ridge width and 1ămm overall length. The ratio of the absorber section length to the gain section length was 1:9 which correspond to a rather short absorber section. The material incorporated is InGaAs forming 15 stacked layers of quantum dots [27]. Growth details can be found in [28]. The device was integrated in a module comprising a fiber pigtail, a microwave port, dc contacts, and a thermoelectric cooler. Basic properties like PIV-curves, repetition frequency, pulse width/pulse shape dependencies on operating parameters, temperature dependencies as well as the characteristics of hybrid ML are already published in [29, 30, 26, 31].

All measurements have been performed at room temperature in passive regime. The light output from the fiber was, after passing an optical isolator, given either to a high speed photodetector or to an autocorrelator. The high speed photodetector was connected to an electrical spectrum analyzer (ESA).

Previous measurements have not revealed any pure Q-switching in this QD mode-locked laser [24]. The reason is that the region of the instability is negligible compared to the ML region. High resolution scans around the lasing threshold show the already seen Q-switched ML (qsml) and closer to the threshold pure Q-switching (qs), see the lower panel in Fig. 10.

In the upper panel of Fig. 10 three examples of electrical spectrum analyzer traces are given showing the evolution of the electrical spectrum with the increase of the injection current for a fixed reverse bias. This panel is an experimental counterpart of the lower panel in Fig. 6. The electrical spectrum analyzer traces are spanning a frequency range from 1MHz up to 42GHz. The resolution bandwidth was set to 100kHz. At low injection currents, close to the laser threshold, only spectral lines at frequencies around 1GHz are visible in the spectrum, see the lower trace in the upper panel of Fig. 10. This corresponds to a pure Q-switching regime. For example, for the absorber bias -8V the Q-switching frequency starts with 0.54GHz for an injection current of 24mA and increases linearly up to 1.36GHz at 30mA of the current (not shown). By fitting the measurement results we have obtained a slope of 0.128GHz/mA for this linear increase. Going back to Fig. 10 we see that by increasing the current further, in this case 2mA, the Q-switching spectral lines become more intense and in addition a spectral line at the fundamental ML frequency appears. The ML spectral line is accompanied by two side peaks with a distance corresponding to the Q-switching frequency. At other operating parameters a pair of additional side peaks have been observed, which correspond to higher harmonics of the Q-switching frequency. A more intense pumping of the gain section results in a pure fundamental ML peak without any side peaks, see the upper trace in the upper panel of Fig. 10. The results of measurements of electrical spectrum traces for absorber voltages between -4 and -8V and injection currents between 15 and 35mA are summarized in the lower panel of Fig. 10. By calculating the difference between the amplitude of the Q-switching peak and

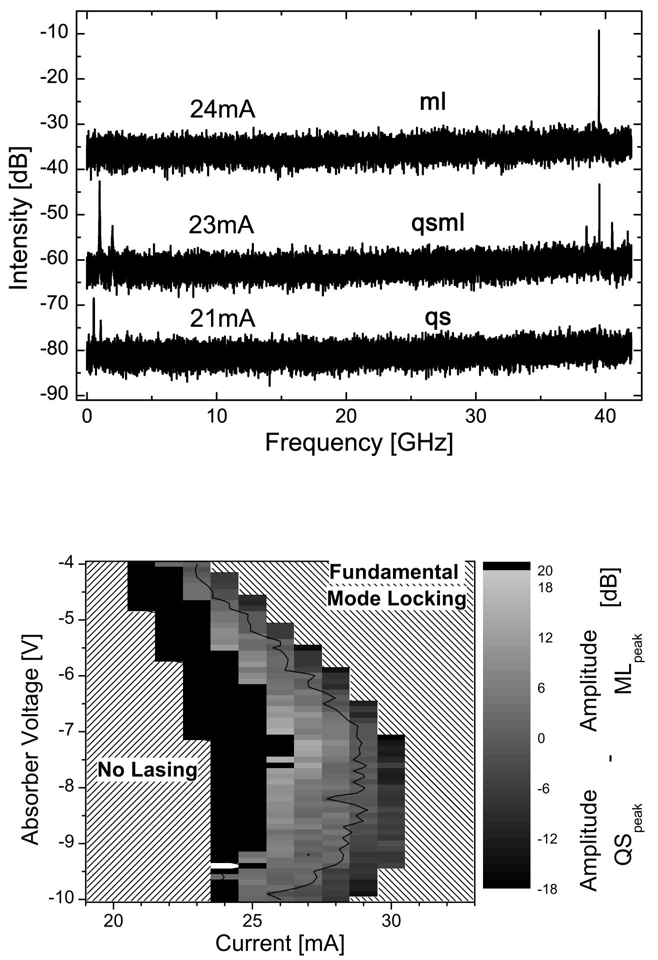

Figure 10: Transition from Q-switching to fundamental ML regime. Top: Electrical spectrum analyzer traces for three different currents at -4V reverse bias. The offset has been shifted for better visibility. qs - Q-switching, qsml - Q-switched ML, and ml - fundamental ML. Bottom: Different gray levels indicate the difference of the Q-switching spectral peak amplitude and the amplitude of the ML peak. Areas were no lasing or fundamental ML takes place are gray striped and labeled. The black region denotes pure Q-switching. The thin black line marks the value “0”, were Q-switching and ML spectral peaks have equal amplitudes.

the amplitude of the fundamental ML peak, the region where Q-switched ML takes place has been identified. Higher harmonics have not been taken into account. The region where only a Q-switching line appears in the electrical spectrum is shown in black. Negative (positive) numbers in the lower panel of Fig. 10 represent the measurements in which the ML line is more (less) intense than the Q-switching one. The thin black line within the gray-coded area in the lower panel of Fig. 10, is a guide to the eyes, showing the parameters where both spectral components, Q-switched and mode-locked, have equal amplitudes. No matter which driving current / absorber voltage combination is used: the pure Q-switching is only present in a range of 3mA (in most cases the range is only 2mA). Compared to the region where proper fundamental ML takes place, e.g. for an absorber voltage of -8V from 30mA to 100mA, this range is less than 4%. This can be seen from the numbered gray scale bars at the bottom of the lower panel of Fig. 11. Besides the evaluation of the electrical spectra, one can gain information about the characteristics of mode-locked pulses by measuring autocorrelation traces, which represent a convolution of a pulse with itself. Details on the limitations of this method and real pulse shapes can be found in [31]. Despite these limitations, the autocorrelation traces can be used for monitoring the evolution of the pulse amplitude with the injection current. One has to keep in mind that the second harmonic generation (SHG) signal amplitude depends quadratically on the input amplitude.

As it is seen from Fig. 11, the peak amplitude of mode-locked pulses increases with the injection current in the range from 30mA to 80mA, above this range it starts to decrease up to 100mA. At even higher injection currents the laser operates in a cw regime. This behavior is similar to that predicted theoretically for the case of short absorber section, see Fig. 5. Although the peak amplitude decreases in the range from 80mA to 100mA, the overall optical output gets steadily higher [29]. This is due to the facts that on one hand the pulses become broader having, therefore, more energy per pulse and on the other hand a cw-background shows up. Unlike the 20GHz QD mode-locked laser studied in [24], no higher harmonics (pulse repetition frequency doubling) has been observed in the 40GHz device using the autocorrelation technique. All other features which are Q-switching, Q-switched ML, fundamental ML, the relation between the regimes as well the behavior of the amplitude with current are in qualitative agreement with the results obtained by simulations.

5 Conclusion

We have studied the effect of carrier exchange processes between quantum dots and 2D reservoir of a QD-in-a well structure on the dynamical behavior of a monolithic mode-locked QD laser. We have presented a bifurcation analysis of the set of delay differential equations governing the time evolution of the electric field envelope, occupation probabilities of the ground state in quantum dots, and carrier densities in the 2D reservoir. In particular, these equations contain Pauli blocking terms which lead to a decrease of the capture rate when the occupation probability of the ground state

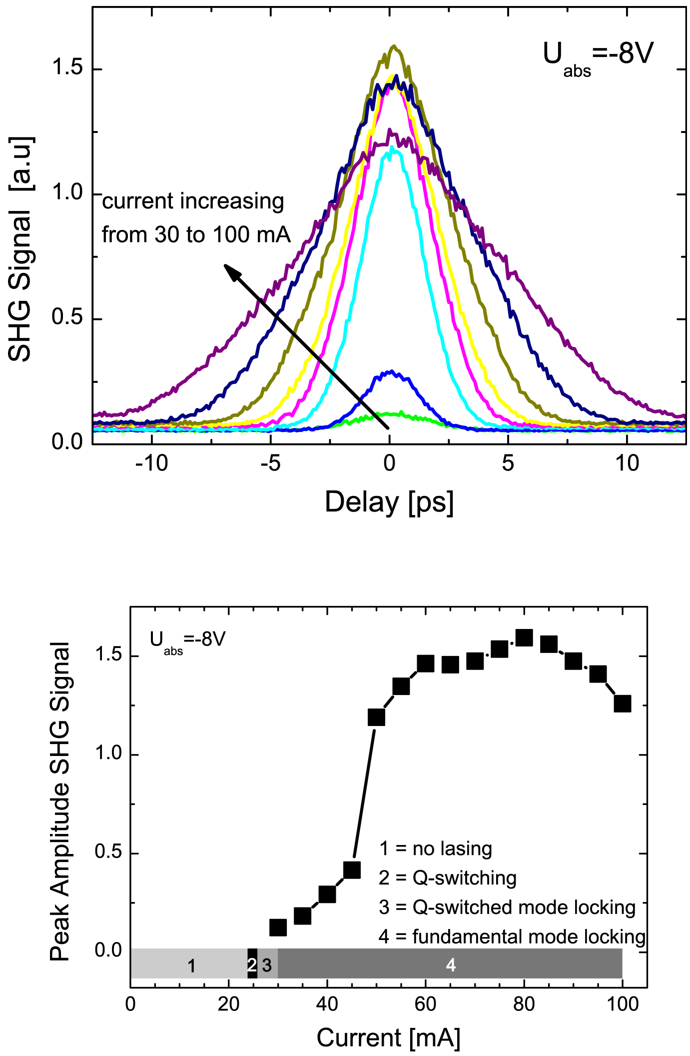

Figure 11: Experimentally measured evolution of the pulse peak amplitude and pulse width with the increase of the injection current. Top: Autocorrelator traces obtained for currents ranging from 30mA to 100mA at a fixed absorber voltage of -8V. Bottom: Evolution of the peak amplitude with injection current extracted from the autocorrelator traces presented in the top figure. The operating regimes shown in Fig. 10 are marked using numbered gray-scale bars.

in the quantum dots increases. We have shown that the dynamical behavior of the laser depends strongly on the relative length of the gain and absorber sections. When the absorber section is relatively long a bistability appears between the zero intensity state and ML regimes. In this case, the Q-switching behavior disappears completely. Another peculiar feature of the traveling wave (1)-(3) and delay differential (4)-(8) QD laser models is the existence of period-doubling bifurcation of the harmonic ML regime with the repetition frequency approximately twice higher than that of the fundamental ML regime. As a result of this bifurcation a regime with two pulses having different amplitudes and separations in time develops. A similar regime was observed experimentally in a 20GHz monolithic QD mode-locked laser [24]. The dynamical behavior of a mode-locked laser with relatively short absorber is qualitatively quite similar to that of the quantum well ML laser model [15, 16, 21, 17, 19]. However, in contrast to the results reported in these papers, apart from Q-switched ML, numerical simulations of Eqs. (4)-(8) have revealed the existence of a pure Q-switching regime at very small injection currents. We have presented experimental evidence of the existence of such a regime in a 40GHz monolithic passively mode-locked QD laser. The relation between the experimentally observed regimes, as well the behavior of the amplitude with the current, are in qualitative agreement with the results obtained by simulations.

6 Acknowledgments

A.G.V. is grateful to E. Avrutin and E.A. Viktorov for useful discussions. The authors from WIAS and TU Berlin acknowledge the funding of this work by the SFB787 of the DFG. D. R. was partially supported by the Federal Programme 'Scientists of Innovative Russia', grant 2009-1.5-507-007.

References

[1] L. A. Jiang, E. P. Ippen, and H. Yokoyama, *Ultrahigh-Speed Optical Transmission Technology* (Springer, 2007), chap. Semiconductor mode-locked lasers as pulse sources for high bit rate data transmission, pp. 21–51.

[2] B. Hüttl, R. Kaiser, C. Kindel, S. Fidorra, W. Rehbein, H. Stolpe, G. Sahin, U. Bandelow, M. Radziunas, A.G.Vladimirov, and H. Heidrich, "Monolithic 40 GHz mqw mode-locked lasers on GaInAsP/InP with low pulse widths and controlled Q-switching," Appl. Phys. Lett. **88**, 221104 (2006).

[3] E. U. Rafailov, M. A. Cataluna, and W. Sibbett, "Mode-locked quantum-dot lasers," Nature Photonics **1**, 395–401 (2007).

[4] Y. Chu, R. V. Penty, and I. H. White, "Measurement of the linewidth enhancement factor of quantum dot lasers using external light injection," in "Pacific Rim Conference on Lasers and Electro-Optics," (Tokyo, Japan, 2005).

[5] M. Kuntz, G. Fiol, M. Lämmlin, D. Bimberg, M. G. Thompson, K. T. Tan, C. Marinelli, R. V. Penty, I. H. White, V. M. Ustinov, A. E. Zhukov, Y. M. Shernyakov, and A. R. Kovsh, "35 GHz mode-locking of 1.3 μm quantum dot lasers," Appl. Phys. Lett. **85**, 843 (2004).

[6] L. Shi, Y. H. Chen, B. Xu, Z. C. Wang, Y. H. Jiao, and Z. G. Wang, "Status and trends of short pulse generation using mode-locked lasers based on advanced quantum-dot active media," J. Phys. D: Appl. Phys. **40**, R307–R318 (2007).

[7] E. U. Rafailov, M. A. Cataluna, W. Sibbett, N. D. Il'inskaya, Y. Zadiranov, A. E. Zhukov, V. M. Ustinov, D. A. Livshits, A. R. Kovsh, and N. N. Ledentsov, "High-power picosecond and femtosecond pulse generation from a two-section mode-locked quantum-dot laser," Appl. Phys. Lett. **87**, 081107 (2005).

[8] M. G. Thompson, A. Rae, R. L. Sellin, C. Marinelli, R. Penty, I. H. White, A. R. Kovsh, S. S. Mikhrin, D. A. Livshits, and I. L. Krestnikov, "Subpicosecond high-power mode locking using flared waveguide monolithic quantum-dot lasers," Appl. Phys. Lett. **88**, 133119 (2006).

[9] V. M. Ustinov, A. E. Zhukov, A. Y. Egorov, and N. A. Maleev, *Quantum Dot Lasers* (Oxford University Press, 2003).

[10] J. Gomis-Bresco, S. Dommers, V. V. Temnov, U. Woggon, J. Martinez-Pastor, M. Laemmlin, and D. Bimberg, "Ingaas dots coupled to a reservoir of nonequilibrium free carriers," IEEE J. Quantum Electron. **45**, 1121–1128 (2009).

[11] A. Markus, J. X. Chen, O. Gauthier-Lafaye, J.-G. Provost, C. Paranthën, and A. Fiore, "Impact of intraband relaxation on the performance of a quantum-dot laser," IEEE J. Sel. Top. Quant. Electron. **9**, 1308–1314 (2003).

[12] A. Markus, M. Rossetti, V. Calligari, D. Chek-Al-Kar, J. X. Chen, A. Fiore, and R. Scollo, "Two-state switching and dynamics in quantum dot two-section lasers," J. Appl. Phys. **100**, 113104 (2006).

[13] D. O'Brien, S. P. Hegarty, G. Huyet, and A. V. Uskov, "Sensitivity of quantum-dot semiconductor lasers to optical feedback," Opt. Lett. **29**, 1–3 (2004).

[14] E. Viktorov, P. Mandel, A.G.Vladimirov, and U. Bandelow, "A model for mode-locking in quantum dot lasers," Appl. Phys. Lett. **88**, 201102 (2006).

[15] A. Vladimirov, D. Turaev, and G. Kozyreff, "Delay differential equations for mode-locked semiconductor lasers," Opt. Lett. **29**, 1221–1223 (2004).

[16] A. Vladimirov and D. Turaev, "Model for passive mode-locking in semiconductor lasers," Phys. Rev. A **72**, 033808 (2005).

[17] D. Rachinskii, A. Vladimirov, U. Bandelow, B. Hüttl, and R. Kaiser, "Q-switching instability in a mode-locked semiconductor laser," J. Opt. Soc. Am. B **23**, 663–670 (2006).

[18] U. Bandelow, H. Wenzel, and H. Wünsche, "Influence of inhomogeneous injection on sidemode suppression in strongly coupled DFB semiconductor lasers," Electron. Lett. **28**, 1324–1326 (1992).

[19] U. Bandelow, M. Radziunas, A. G. Vladimirov, B. Hüttl, and R. Kaiser, "40 GHz modelocked semiconductor lasers: Theory, simulations and experiment," Optical and Quantum Electronics **38**, 495–512 (2006).

[20] A. G. Vladimirov, A. S. Pimenov, and D. Rachinskii, "Numerical study of dynamical regimes in a monolithic passively mode-locked semiconductor laser," IEEE Journal of Quantum Electronics **45**, 462–468 (2009).

[21] A. Vladimirov and D. Turaev, "New model for mode-locking in semiconductor lasers," Radiophys. & Quant. Electron. **47**, 857–865 (2004).

[22] K. Engelborghs, T. Luzyanina, and G. Samaey, "DDE-BIFTOOL V. 2.00: A matlab package for bifurcation analysis of delay differential equations," Tech. Rep. TW-330, Department of Computer Science, K.U.Leuven, Leuven, Belgium (2001).

[23] N. Guglielmi and E. Hairer, *Users' Guide for the Code RADAR5* (2000).

[24] E. Viktorov, P. Mandel, M. Kuntz, G. Fiol, D. Bimberg, A. G. Vladimirov, and M. Wolfrum, "Stability of the modelocked regime in quantum dot lasers," Appl. Phys. Lett. **91**, 231116 (2007).

[25] F. Kärtner, J. A. der Au, and U. Keller, "Mode-locking with slow and fast saturable absorbers – what is the difference," IEEE J. Sel. Top. Quantum Electron. **4**, 159–168 (1998).

[26] G. Fiol, D. Arsenijević, D. Bimberg, A. G. Vladimirov, M. Wolfrum, E. A. Viktorov, and P. Mandel, "Hybrid mode-locking in a 40 GHz monolithic quantum dot laser," Appl. Phys. Lett. **96**, 1429–1435 (2010).

[27] D. Bimberg, "Quantum dot based nanophotonics and nanoelectronics," Electronics Letters **44(3)**, 168–170 (2008).

[28] A. R. Kovsh, N. A. Maleev, A. E. Zhukov, S. S. Mikhrin, A. P. Vasil'ev, E. A. Semenova, Y. M. Shernyakov, M. V. Maximov, D. A. Livshits, V. M. Ustinov, N. N. Ledentsov, D. Bimberg, and Z. I. Alferov, "InAs/InGaAs/GaAs quantum dot lasers of 1.3 m range with enhanced optical gain," Journal of Crystal Growth **251**, 729–736 (2003).

[29] M. Kuntz, G. Fiol, M. Laemmlin, C. Meuer, and D. Bimberg, "High-speed mode-locked quantum-dot lasers and optical amplifiers," Proceedings of the IEEE **95**, 1767–1778 (2007).

[30] G. Fiol, C. Meuer, H. Schmeckebier, D. Arsenijević, S. Liebich, M. Laemmlin, M. Kuntz, and D. Bimberg, "Quantum-dot semiconductor mode-locked lasers and amplifiers at 40 GHz," IEEE Journal of Quantum Electronics **45**, 1429–1435 (2009).

[31] H. Schmeckebier, G. Fiol, C. Meuer, D. Arsenijević, and D. Bimberg, “Complete pulse characterization of quantum-dot mode-locked lasers suitable for optical communication up to 160 Gbit/s,” Optics Express **18**, 3415–3425 (2010).